













# Interpolating individual line-of-sight neutron spectrometer measurements onto the “sky” at the National Ignition Facility (NIF)

Cite as: Rev. Sci. Instrum. 92, 043512 (2021); <https://doi.org/10.1063/5.0040590>

Submitted: 14 December 2020 . Accepted: 15 March 2021 . Published Online: 02 April 2021

 E. P. Hartouni,  R. M. Bionta,  D. T. Casey, M. J. Eckart,  M. Gatu-Johnson,  G. P. Grim,  K. D. Hahn,  J. Jeet, S. M. Kerr,  A. L. Kritcher, B. J. MacGowan,  A. S. Moore,  D. H. Munro,  D. J. Schlossberg, and  A. Zylstra





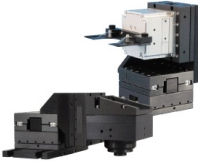
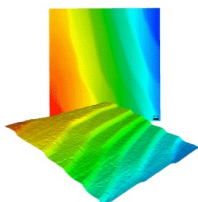
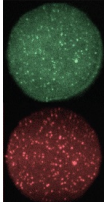
View Online



Export Citation



CrossMark

 <p>MAD CITY LABS INC. www.madcitylabs.com</p>	<p>Nanopositioning Systems</p> 	<p>Modular Motion Control</p> 	<p>AFM and NSOM Instruments</p> 	<p>Single Molecule Microscopes</p> 
---	--	--	---	--

# Interpolating individual line-of-sight neutron spectrometer measurements onto the “sky” at the National Ignition Facility (NIF)

Cite as: Rev. Sci. Instrum. 92, 043512 (2021); doi: 10.1063/5.0040590

Submitted: 14 December 2020 • Accepted: 15 March 2021 •

Published Online: 2 April 2021

















View Online



Export Citation



CrossMark

E. P. Hartouni,<sup>1,a)</sup>  R. M. Bionta,<sup>1</sup>  D. T. Casey,<sup>1</sup>  M. J. Eckart,<sup>1</sup> M. Gatu-Johnson,<sup>2</sup>  G. P. Grim,<sup>1</sup>   
K. D. Hahn,<sup>1</sup>  J. Jeet,<sup>1</sup>  S. M. Kerr,<sup>1</sup>  A. L. Kritcher,<sup>1</sup>  B. J. MacGowan,<sup>1</sup>  A. S. Moore,<sup>1</sup>  D. H. Munro,<sup>1,b)</sup>   
D. J. Schlossberg,<sup>1</sup>  and A. Zylstra<sup>1</sup> 

## AFFILIATIONS

<sup>1</sup>Lawrence Livermore National Laboratory, Livermore, California 94550, USA

<sup>2</sup>Plasma Science and Fusion Center, Massachusetts Institute of Technology, Cambridge, Massachusetts 02139, USA

**Note:** Paper published as part of the Special Topic on Proceedings of the 23rd Topical Conference on High-Temperature Plasma Diagnostics.

<sup>a)</sup> Author to whom correspondence should be addressed: hartouni1@llnl.gov

<sup>b)</sup> Retired.

## ABSTRACT

Nuclear diagnostics provide measurements of inertial confinement fusion implosions used as metrics of performance for the shot. The interpretation of these measurements for shots with low mode asymmetries requires a way of combining the data to produce a “sky map” where the individual line-of-sight values are used to interpolate to other positions in the sky. These interpolations can provide information regarding the orientation of the low mode asymmetries. We describe the interpolation method, associated uncertainties, and correlations between different metrics, e.g.,  $T_{\text{ion}}$ , down scatter ratio, and hot-spot velocity direction. This work is also related to recently reported studies [H. G. Rinderknecht *et al.*, Phys. Rev. Lett. **124**, 145002 (2020) and K. M. Woo *et al.*, Phys. Plasmas **27**, 062702 (2020)] of low mode asymmetries. We report an analysis that makes use of a newly commissioned line of sight, a scheme for incorporating multiple neutron spectrum measurement types, and recent work on the sources of implosion asymmetry to provide a more complete picture of implosion performance.

Published under license by AIP Publishing. <https://doi.org/10.1063/5.0040590>

## I. INTRODUCTION

Inertial confinement fusion (ICF) results from the conversion of capsule ablation in a high temperature radiation field into radial compression providing PdV work to increase the temperature of the DT fuel contained within the capsule.<sup>1–4</sup> The coupling of the PdV work to the fuel compression depends on the symmetry of the implosion with asymmetric components not contributing to the increased temperatures.<sup>5</sup> Diagnosing implosion performance must include an assessment of low mode asymmetries when comparing to predictions of implosion metrics.<sup>6</sup>

Exploring the effect of laser drive “up–down” asymmetry on the NIF<sup>7,8</sup> in two dimensions leads to a characterization of the capsule response in terms of a spectrum of perturbations described as a Legendre polynomial. The expansion terms of interest to this study have indices 0 and 1 and are referred to as a “mode 0” or  $4\pi$  isotropic term

and a “mode 1” term, which is anisotropic. This computational study made predictions regarding the angular dependence, which are the subject of this study: (1) the burning plasma common velocity,  $v_{\text{h.s.}}$ , indicates the direction of the perturbation; (2) ion temperature  $T_{\text{ion}}$  has an angular distribution that varies as  $\cos^2 \xi$  defined with respect to the perturbation direction; and (3) the fuel shell areal density,  $\rho R$ , has an angular distribution that varies as  $-\cos \xi$  defined with respect to the perturbation direction (that is, low  $\rho R$  in the direction of  $v_{\text{h.s.}}$  and high  $\rho R$  away).

A suite of neutron diagnostics exists to measure these three quantities: burning plasma common velocity (hot-spot velocity),  $v_{\text{h.s.}}$ ,<sup>9,10</sup> ion temperature,  $T_{\text{ion}}$ ; and the down-scattered ratio.<sup>11–13</sup> These neutron diagnostics are positioned at the NIF along independent line-of-sight (LOS) directions shown in Fig. 1, and the work reported here combines these measurements into a three dimensional reconstruction describing the interpolation of the measured

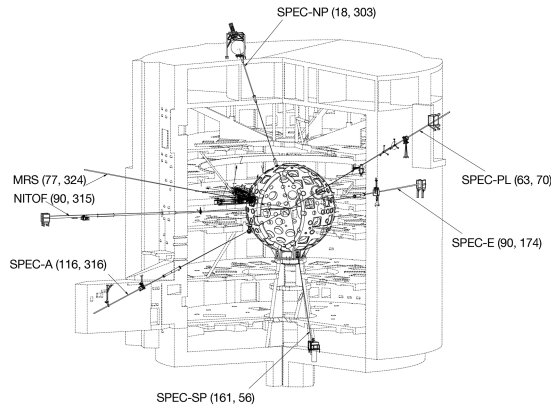


**FIG. 1.** Neutron spectrometer system at the NIF. The seven line-of-sight measurements, six using neutron time-of-flight and one using neutron energy, are arranged around the target chamber system. The time-of-flight systems are roughly 20 m from the Target Chamber Center (TCC). The system of spectrometers can be used to determine three dimensional features of imploding ICF capsules.

quantities to all angles and infers directional information related to mode 1 perturbations testing the calculations.

## II. OBSERVABLES

Each line-of-sight neutron spectrometer reports the three quantities of interest:  $v_{\text{LOS}}$ ,  $T_{\text{ion}}$ , and DSR (down-scattered ratio). These spectroscopic observables are connected to the underlying plasma variables: “thermal” ion temperature, ion kinetic energy, and plasma velocity, which are an average over the plasma in space and time weighed by the ion reactivity, the so-called “burn-weighted average” measured by the spectrometers<sup>14</sup> (denoted by the brackets  $\langle \cdot \rangle$ ). The analysis measures the *shift* of the mean neutron kinetic energy,

$$\langle \omega_{\text{LOS}} \rangle = \langle u_{\parallel} \rangle + \langle \bar{\kappa} \rangle + \frac{2 + \beta_0^2}{2v_0} \langle \tau \rangle + \dots, \quad (1)$$

where  $u_{\parallel}$  is the center-of-momentum motion of the fusing ion pair in the direction of the LOS,  $\bar{\kappa}$  is the shift due to the burn averaged kinetic energy distribution of the reacting ions, and  $\tau$  is the ion thermal temperature in units of velocity squared. The neutron velocity  $v_0$  is taken to be 51 233.5920(34) km/s for DT fusion and 21 601.8596(77) km/s for DD fusion (using the CODATA 2010 values<sup>15</sup>). The relativistic velocity  $\beta_0 = v_0/c$ , where  $c$  is the speed-of-light. Higher order terms are neglected in this analysis.

$T_{\text{ion}}$  is associated with the variance of the neutron kinetic energy distribution,

$$\text{Var}(\omega_{\text{LOS}}) = \langle \tau \rangle + \text{Var}(u_{\parallel}) + \dots, \quad (2)$$

which shows the source of departure of the neutron variance from the burn averaged ion thermal temperature where the plasma velocity variance is large.<sup>16</sup>

The down scatter ratio (DSR) is the integral of the neutron spectrum between 10 and 12 MeV to 13–15 MeV. The neutrons produced by fusion reactions in the plasma will be transmit through a high areal density region composed of the DT fuel layer and the remaining C, CH, or Be capsule. These neutrons can undergo elastic

scattering through angles that put them along the detector LOS but with reduced energy,

$$\cos \theta^{\text{CM}} \approx 1 - \frac{1}{2} \left( 1 - \frac{K'_n}{K_n} \right) \frac{M}{m_n} \left( 1 + \frac{m_n}{M} \right)^2, \quad (3)$$

which holds for  $K_n \ll Mc^2$ , where  $K_n$  and  $K'_n$  are the kinetic energy of the incident and scattered neutron,  $m_n$  is the neutron mass, and  $M$  is the scattering ion mass.  $\cos \theta^{\text{CM}}$  is the scattering angle in the center-of-mass of the neutron–ion system. Equation (3) shows that the scattered neutron kinetic energy scatters through a unique angle. When projected along a particular LOS from the center of the sphere, the area included in the neutrons scattered between 10 and 12 MeV forms an annulus on a spherical surface that extends from  $47^\circ$  to  $69^\circ$  for scattering on D and from  $52^\circ$  to  $76^\circ$  for T, and these are shown, combined, in Fig. 2(a).

The scattered neutron intensity can be considered a convolution of the neutron “birth spectrum” with the differential scattering cross section,

$$I_{\text{scat}}(K'_n) = \int_{K'_n}^{\infty} dK_n \frac{d\Omega}{dK_n} I_{\text{birth}}(K_n) \frac{d\sigma}{d\Omega}(\cos \theta^{\text{CM}}), \quad (4)$$

where there is a term for each scattering ion. For this analysis, we consider scattering from T and D only, where there are equal number of atoms for the two ion species. There are additional complications in distribution of the neutron emission and the areal density of the fuel shell due to thickness variation. Combining these various distributions will blur out the scattering annulus into a disk for neutrons originating from fusions distributed throughout the hot-spot. The resulting region is shown in Fig. 2(b). For each measurement, these disks have a  $60^\circ$  angular extent from the LOS direction and can

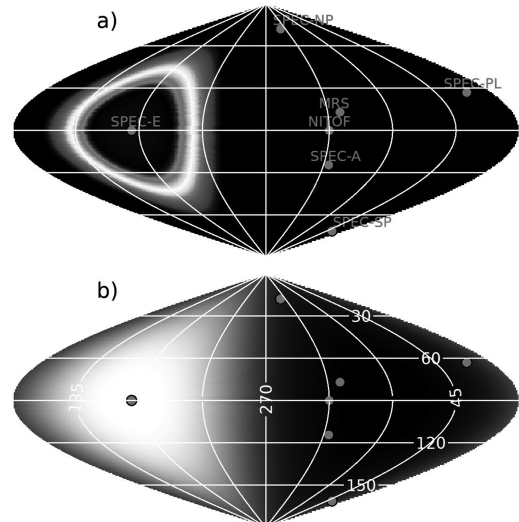


**FIG. 2.** Area of the NIF “sky” sampled by the SPEC-E down-scattered neutrons. Lighter areas show the relative density of down-scattered neutrons. (a) shows the space for a point source at the origin and (b) a distributed source. The extended nature of the “sky” sampled by a LOS DSR measurement requires the overlapping regions to be treated in the optimization. This is done using the correlations described in Table I.

**TABLE I.** Correlations of DSR measurements between pairs of detector LOS directions (named as in Fig. 1). The columns indicate the correlations found in experimental data (“expt.” using the Pearson correlation between the different LOS measurements for the entire layered implosion database) and calculated for the distributed (“dist.”) and point source models. The experimental data trend closer to the distributed source model.

Pair		Expt.	Dist.	Point
SPEC-NP	MRS	0.673	0.735	0.214
SPEC-NP	SPEC-E	0.357	0.422	0.071
SPEC-NP	NITOF	0.587	0.643	0.244
SPEC-NP	SPEC-A	0.582	0.453	0.114
SPEC-NP	SPEC-SP	0.443	0.131	0.000
MRS	SPEC-E	0.491	0.168	0.000
MRS	NITOF	0.899	0.979	0.603
MRS	SPEC-A	0.805	0.884	0.266
MRS	SPEC-SP	0.672	0.408	0.053
SPEC-E	NITOF	0.560	0.193	0.000
SPEC-E	SPEC-A	0.613	0.205	0.000
SPEC-E	SPEC-SP	0.691	0.441	0.097
NITOF	SPEC-A	0.890	0.948	0.389
NITOF	SPEC-SP	0.764	0.478	0.152
SPEC-A	SPEC-SP	0.836	0.667	0.232

overlap with disks associated with other LOS directions. The overlapping regions correlate one measurement to another, and to fit the DSR measurements it is required to properly account for the correlations. Table I shows the correlations found in layered DT implosions on the NIF and the calculations assuming a uniform scattering layer and either a distributed or a point source model.

### III. INTERPOLATION

Angular variations in the plasma velocity variance and DSR aligned with the hot-spot velocity are predicted<sup>7</sup> for mode 1 capsule drive perturbations. These variations will be measured along each of the LOS, and these measurements can be used along with a model of the angular variations for each observable. The hot-spot velocity in Eq. (1) suggests that the LOS velocity is

$$v_{\text{LOS}} = \tilde{v}_{\text{h.s.}} \cdot \hat{n}_{\text{LOS}} + v_{\text{iso}}, \quad (5)$$

where the first term on the rhs corresponds to the first term in Eq. (1), with  $\tilde{v}_{\text{h.s.}}$  being the hot-spot velocity vector and  $\hat{n}_{\text{LOS}}$  being the LOS unit direction vector. The second term,  $v_{\text{iso}}$ , the isotropic velocity, corresponds to the second and third terms of Eq. (1) associated with the temperature dependent shift of the mean neutron kinetic energy distribution. The  $T_{\text{ion}}$  distribution follows Eq. (2),

$$T_{\text{ion}}(\theta, \phi) = T_0 + \Delta T \cos^2 \xi(\theta_0, \phi_0, \theta, \phi), \quad (6)$$

where the angle  $\xi$  is defined by the  $T_{\text{ion}}$  axis of azimuthal symmetry (an assumption of this model) and some sky locations (e.g., the  $i$ th LOS directions),

$$\cos \xi(\theta_0, \phi_0, \theta_i, \phi_i) = \hat{n}_{\text{a.s.}} \cdot \hat{n}_{\text{LOS}}, \quad (7)$$

where the axis of symmetry is defined by the unit vector,

$$\hat{n}_{\text{a.s.}} = (\sin \theta_0 \cos \phi_0, \sin \theta_0 \sin \phi_0, \cos \theta_0). \quad (8)$$

The dot product expands to

$$\begin{aligned} \cos \xi &= \sin \theta_0 \cos \phi_0 \sin \theta_i \cos \phi_i + \sin \theta_0 \sin \phi_0 \sin \theta_i \sin \phi_i \\ &\quad + \cos \theta_0 \cos \theta_i, \end{aligned} \quad (9)$$

where  $(\theta_i, \phi_i)$  is the direction of the LOS. The four parameters  $T_0, \Delta T, \theta_0,$  and  $\phi_0$  describe the angular distribution of  $T_{\text{ion}}$ .

The DSR angular dependence is described by

$$\text{DSR}(\theta, \phi) = \sum_{L=0}^1 \sum_{M=-L}^L a_{L,M} Y_{L,M}(\theta, \phi), \quad (10)$$

a truncated spherical harmonic expansion. The four parameters  $a_{0,0}, a_{1,-1}, a_{1,0},$  and  $a_{1,1}$  define the DSR sky.

The expressions for the hot-spot velocity,  $T_{\text{ion}}$ , and DSR in Eqs. (5), (6), and (10) are chosen to be described by four parameters because of the limited number of LOS measurements available and the desire to describe an effective “direction” for the variation. The DSR variation at  $L = 0, 1$  can be described as the direction defined by the maximum and minimum DSR values interpolated in the DSR sky.

### IV. OPTIMIZATION

Given the LOS measurements, the parameters to the three quantities hot-spot velocity  $v_{\text{LOS}}$ ,  $T_{\text{ion}}$ , and DSR are found by optimizing the  $\chi^2$  formed by the interpolation formula,

$$\text{LSQ} = (\mathbf{w} - \mathbf{G}\mathbf{v})^\top (\mathbf{w} - \mathbf{G}\mathbf{v}), \quad (11)$$

where  $\mathbf{w}$  is the vector of  $v_{\text{LOS}}$  measurements,  $\mathbf{v} = [u_x, u_y, u_z, v_{\text{iso}}]$  is the hot-spot velocity 4-vector, and  $\mathbf{G}$  is the projection into the LOS directions,

$$\mathbf{G} = \begin{pmatrix} \cos \phi_1 \sin \theta_1 & \sin \phi_1 \sin \theta_1 & \cos \theta_1 & 1 \\ \cos \phi_2 \sin \theta_2 & \sin \phi_2 \sin \theta_2 & \cos \theta_2 & 1 \\ \vdots & \vdots & \vdots & \vdots \\ \cos \phi_N \sin \theta_N & \sin \phi_N \sin \theta_N & \cos \theta_N & 1 \end{pmatrix}.$$

The  $T_{\text{ion}}$  parameters

$$\chi^2 = \sum_i \frac{1}{\sigma_i^2} [T_i - T_0 - \Delta T \cos^2 \xi(\theta_0, \phi_0, \theta, \phi)]^2, \quad (12)$$

where  $T_i$  and  $\sigma_i$  are the LOS measured  $T_{\text{ion}}$  and its uncertainty, respectively. In addition, the DSR optimization

$$\begin{aligned} \chi^2 &= \sum_{ij} \left[ \text{DSR}_i - \sum_{L,M} a_{L,M} Y_{L,M} \right] \text{COV}_{ij} \\ &\quad \times \left[ \text{DSR}_j - \sum_{L,M} a_{L,M} Y_{L,M} \right], \end{aligned} \quad (13)$$

where  $\text{DSR}_i$  and  $\sigma_i^2$  are the LOS measured DSR and its uncertainty, respectively. The matrix  $\text{COV}_{ij}$  captures the covariance of the measurements, which includes the correlation matrix  $\rho_{ij}$ , given in Table I,

$$\text{COV}_{ij} = \frac{\rho_{ij}}{\sigma_i^2 \sigma_j^2}. \quad (14)$$

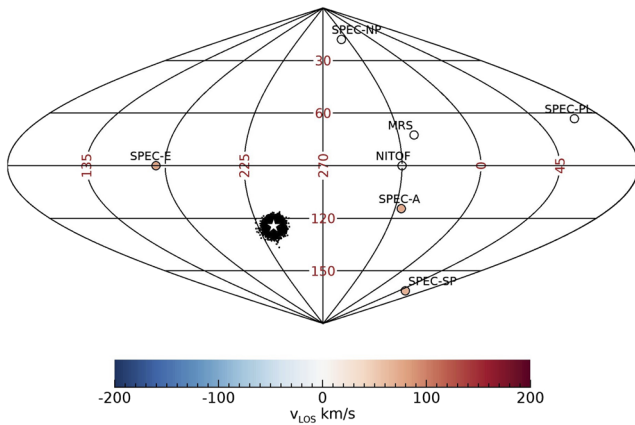


**FIG. 3.** Hot-spot velocity for shot N190918-001. The LOS locations are color coded to indicate the LOS velocity from the quartz Cherenkov detector (QCD) system. (NITOF, MRS, and SPEC-PL did not provide data.) The “star” symbol locates the velocity direction at  $(\theta = 125 \pm 2^\circ, \phi = 236 \pm 3^\circ)$  with a velocity magnitude of  $(97 \pm 5)$  km/s and an isotropic velocity of  $(41 \pm 2)$  km/s. The point cloud indicates the results of introducing random Gaussian noise on the LOS velocities with  $\sigma = 5$  km/s matching the QCD performance.

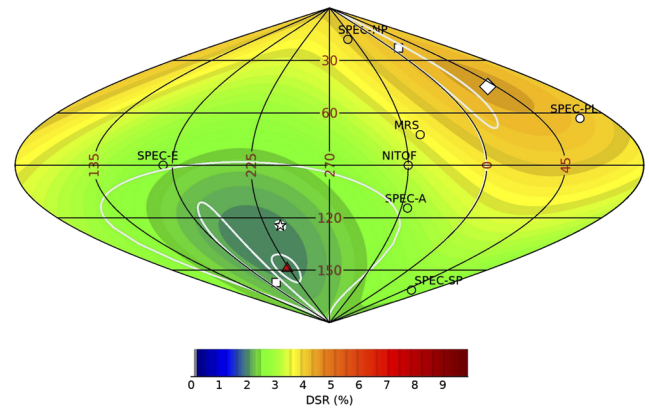


**FIG. 5.** DSR sky for shot N190918-001. The LOS locations are color coded to indicate the LOS DSR measurements. (SPEC-PL did not provide data.) The “star” symbol locates the velocity direction, with  $1\sigma$  error contour, as shown in Fig. 3. The “box” symbols indicate the axis of symmetry for the  $T_{\text{ion}}$  distribution, as shown in Fig. 4. The “diamond” symbol indicates the maximum DSR value location. The antipodal direction is indicated by a large  $1\sigma$  contour. The three independent measures of mode 1 agree with each other and with the expectations of “drive asymmetries” (shown as the red “triangle” symbol) as discussed in the text. The “ $4\pi$ ” DSR value is  $a_{0,0} = (3.2 \pm 0.4)\%$  from Eq. (10).

This treatment estimates the shot-by-shot differences in the correlations occurring through the actual shell by the approximation of a uniform shell that on average varies by less than 10%.

## V. RESULTS

The analysis is applied to the NIF shot N190918-001, a cryo-layered shot of the “HyE” ICF campaign.<sup>17</sup> Figure 3 shows the result of the hot-spot velocity measurements fit to the LOS velocities. In this fit, four parameters are determined by four measurements. Additional measurements (primarily from NITOF and SPEC-PL)

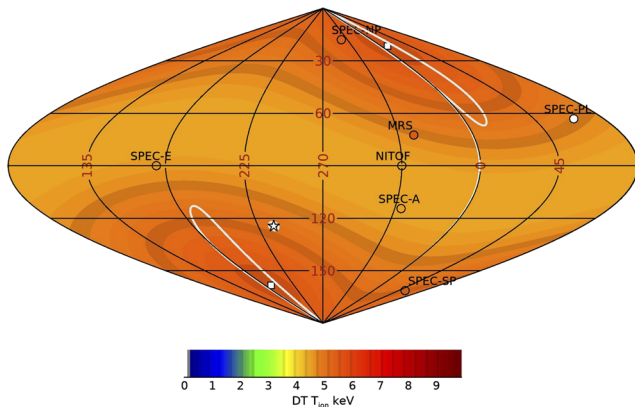


**FIG. 4.**  $T_{\text{ion}}$  sky for shot N190918-001. The LOS locations are color coded to indicate the LOS  $T_{\text{ion}}$ . (SPEC-PL did not provide data.) The “star” symbol locates the velocity direction, with  $1\sigma$  error contour, as shown in Fig. 3. The “box” symbols indicate the axis of symmetry for the distribution, with  $1\sigma$  error contour. This map is a proxy for asymmetric plasma velocity variance and shows increased  $T_{\text{ion}}$  (velocity variance) aligned with the axis. The “ $4\pi$ ”  $T_0 = 4.28 \pm 0.11$  keV from Eq. (6), with a  $\Delta T = 1.37 \pm 0.17$  keV.

will provide a means of using the  $\chi^2$  value as a test of the hot-spot velocity model.

The  $T_{\text{ion}}$  sky is shown in Fig. 4 and shows the expected large velocity variance roughly aligned with the hot-spot velocity.

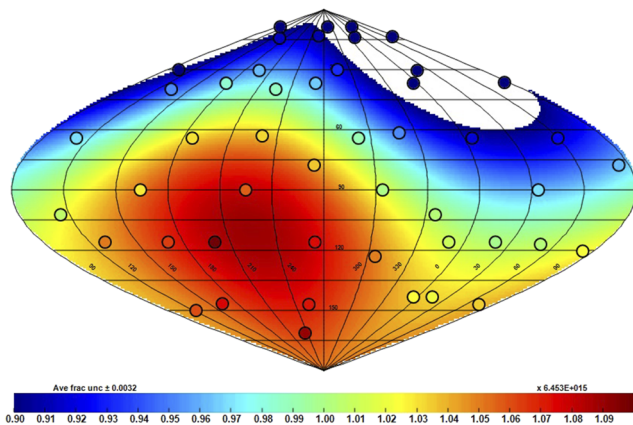
The DSR sky shown in Fig. 5 captures the three determinations of mode 1 perturbations discussed above. The general signature is the hot-spot velocity, the direction of which indicates an axis of symmetry for both the DSR distribution, which is “anti-aligned,” and the  $T_{\text{ion}}$  distribution, which peaks along the axis. The net capsule drive asymmetry derived from the laser, diagnostics windows, ice layer, and ablator is shown as the red triangle symbol.<sup>18</sup> The correspondence of these independent analyses provides evidence that supports the mode 1 perturbation model.

Table II shows the directions from each of the four independent analyses. Combining the directions from the three observables shows an agreement with the average directions  $\delta\theta_0 = 13^\circ$  and  $\delta\phi_0 = 18^\circ$ , whereas combining these directions with the calculated perturbation direction shows an agreement with  $\delta\theta_0 = 12^\circ$  and  $\delta\phi_0 = 16^\circ$ . The large mode 1 perturbation for shot N190918-001 is

**TABLE II.** Summary of the axis of symmetry directions for the four independent analyses. The uncertainties are taken from the  $1\sigma$  variation in the optimization. The combined averages use the rms as an indication of the variation of the results.

Analysis	$\theta_0$	$\phi_0$
Hot-spot velocity	$125 \pm 2^\circ$	$235 \pm 3^\circ$
$T_{\text{ion}}$	$157 \pm 46^\circ$	$192 \pm 11^\circ$
DSR	$135 \pm 47^\circ$	$219 \pm 103^\circ$
Average	$139 \pm 13^\circ$	$215 \pm 18^\circ$
Drive asymmetries	$149 \pm 9^\circ$	$223 \pm 12^\circ$
Average all	$142 \pm 12^\circ$	$217 \pm 16^\circ$





**FIG. 6.** RTNAD sky for shot N190918-001. The LOS locations are color coded to indicate the LOS neutron activation relative to the  $a_{0,0}$  coefficient in the expansion. The color bar range cuts off at  $1 \pm 0.1$ . The region at the “north pole” shows a greatly reduced activation that corresponds with the increased DSR indicated in Fig. 5.

attributed to a large ablator capsule mode 1, which was determined (after the shot) by the inspection data for the specific capsule.

## VI. DISCUSSION

The RTNAD diagnostics at the NIF<sup>19</sup> provide a check of the DSR sky map shown in Fig. 5. The RTNADs measure the neutron activation along 40 LOS directions and show a *decreased* activation in regions of high DSR. The RTNAD sky map fit to a spherical harmonic expansion to  $L = 2$  is shown in Fig. 6. The regions of high and low activation correspond to the DSR map low and high regions from Fig. 5. This correspondence suggests the possibility of including more diagnostics into a simultaneous fit of the mode 1 perturbation analysis, such as the RTNAD. The model for such an analysis would constraint the various diagnostic reference system axes to be the same. The inclusion of the RTNAD data as well as the drive asymmetry data coupled with the model for drive asymmetry could be used to increase the precision of the signatures of mode 1 perturbations and provide insight into capsule implosion performance. Building a “mode 1 model” including the relationship among the parameters<sup>7</sup> of Eqs. (5)–(10) would provide a classification of shots that are consistent with a mode 1 model and inconsistent with the model, which provides valuable diagnostic data for assessing shot performance.

## ACKNOWLEDGMENTS

Lawrence Livermore National Laboratory is operated by Lawrence Livermore National Security, LLC, for the U.S. Department of Energy, National Nuclear Security Administration, under Contract No. DE-AC52-07NA27344. This article (Grant No. LLNL-PROC-817440) was prepared as an account of work sponsored by an agency of the U.S. Government. Neither the U.S. Government nor Lawrence Livermore National Security, LLC, nor any of their employees make any warranty, expressed or implied, or assume any

legal liability or responsibility for the accuracy, completeness, or usefulness of any information, apparatus, product, or process disclosed, or represent that its use would not infringe privately owned rights. The views and opinions of authors expressed herein do not necessarily state or reflect those of the U.S. Government or Lawrence Livermore National Security, LLC, and shall not be used for advertising or product endorsement purposes.

## DATA AVAILABILITY

The data that support the findings of this study are available from the corresponding author upon reasonable request.

## REFERENCES

- H. G. Rinderknecht, D. T. Casey, R. Hatarik, R. M. Bionta, B. J. MacGowan, P. Patel, O. L. Landen, E. P. Hartouni, and O. A. Hurricane, *Phys. Rev. Lett.* **124**, 145002 (2020).
- K. M. Woo, R. Betti, O. M. Mannion, C. J. Forrest, J. P. Knauer, V. N. Goncharov, P. B. Radha, D. Patel, V. Gopalaswamy, and V. Y. Glebov, *Phys. Plasmas* **27**, 062702 (2020).
- S. Atzeni and J. Meyer-ter-Vehn, *The Physics of Inertial Fusion*, International Series of Monographs on Physics (Oxford University Press, 2004).
- J. D. Lindl, *Inertial Confinement Fusion: The Quest for Ignition and Energy Gain Using Indirect Drive* (American Institute of Physics, 1998).
- P. T. Springer, O. A. Hurricane, J. H. Hammer, R. Betti, D. A. Callahan, E. M. Campbell, D. T. Casey, C. J. Cerjan, D. Cao, E. Dewald, L. Divol, T. Doepfner, M. J. Edwards, J. E. Field, C. Forrest, J. Frenje, J. A. Gaffney, M. Gatu-Johnson, V. Glebov, V. N. Goncharov, G. P. Grim, E. Hartouni, R. Hatarik, D. E. Hinkel, L. Berzak Hopkins, I. Igumenshchev, P. Knapp, J. P. Knauer, A. L. Kritcher, O. Landen, A. Pak, S. Le Pape, T. Ma, A. G. MacPhee, D. H. Munro, R. C. Nora, P. K. Patel, L. Peterson, P. B. Radha, S. P. Regan, H. Rinderknecht, C. Sangster, B. K. Spears, and C. Stoeckl, *Nucl. Fusion* **59**(3), 032009 (2018).
- O. A. Hurricane, D. T. Casey, O. Landen, A. L. Kritcher, R. Nora, P. K. Patel, J. A. Gaffney, K. D. Humbird, J. E. Field, M. K. G. Kruse, J. L. Peterson, and B. K. Spears, *Phys. Plasmas* **27**(6), 062704 (2020).
- B. K. Spears, M. J. Edwards, S. Hatchett, J. Kilkenny, J. Knauer, A. Kritcher, J. Lindl, D. Munro, P. Patel, H. F. Robey, and R. P. J. Town, *Phys. Plasmas* **21**(4), 042702 (2014).
- D. J. Schlossberg, G. P. Grim, D. T. Casey, A. S. Moore, R. Nora, B. Bachmann, L. R. Benedetti, R. M. Bionta, M. J. Eckart, J. E. Field, D. N. Fittinghoff, M. Gatu-Johnson, V. Geppert-Kleinrath, E. P. Hartouni, R. Hatarik, W. W. Hsing, L. C. Jarrott, S. F. Khan, J. D. Kilkenny, O. L. Landen, B. J. MacGowan, A. J. Mackinnon, K. D. Meaney, D. H. Munro, S. R. Nagel, A. Pak, P. K. Patel, B. K. Spears, and P. L. Volegov, “Observations of hydrodynamic flows in imploding fusion plasmas on the NIF” (unpublished) (2020).
- M. Gatu-Johnson, D. T. Casey, J. A. Frenje, C. K. Li, F. H. Séguin, R. Petrasso, R. Ashabanner, R. Bionta, S. LePape, M. McKernan, and A. Mackinnon, *Phys. Plasmas* **20**(4), 042702 (2013).
- R. Hatarik, R. C. Nora, B. K. Spears, M. J. Eckart, G. P. Grim, E. P. Hartouni, A. S. Moore, and D. J. Schlossberg, *Rev. Sci. Instrum.* **89**(10), 101138 (2018).
- R. Hatarik, D. B. Sayre, J. A. Caggiano, T. Phillips, M. J. Eckart, E. J. Bond, C. Cerjan, G. P. Grim, E. P. Hartouni, J. P. Knauer, J. M. Mcnane, and D. H. Munro, *J. Appl. Phys.* **118**(18), 184502 (2015).
- G. Grim, G. Morgan, R. Aragonéz, T. Archuleta, D. Bower, C. Danly, O. Drury, J. Dzenitis, V. Fotherley, B. Felker, and D. Fittinghoff, *Proc. SPIE* **8854**, 88540G (2013).
- M. Gatu Johnson, J. A. Frenje, C. K. Li, F. H. Séguin, R. D. Petrasso, R. M. Bionta, D. T. Casey, J. A. Caggiano, R. Hatarik, H. Y. Khater, D. B. Sayre, J. P. Knauer, T. C. Sangster, H. W. Herrmann, and J. D. Kilkenny, *Rev. Sci. Instrum.* **85**, 11E104 (2014).

- <sup>14</sup>D. H. Munro, *Nucl. Fusion* **56**, 036001 (2016).
- <sup>15</sup>P. J. Mohr, B. N. Taylor, and D. B. Newell, *Rev. Mod. Phys.* **84**, 1527 (2012).
- <sup>16</sup>T. J. Murphy, *Phys. Plasmas* **21**, 072701 (2014).
- <sup>17</sup>A. Kritcher, "Achieving record hot spot energies with the largest HDC implosions on NIF in HYBRID-E," in 62nd Annual Meeting of the APS Division of Plasma Physics, 2020.
- <sup>18</sup>B. MacGowan, O. Landen, D. T. Casey, C. Young, P. Michel, D. Callahan, J. M. Di Nicola, D. Mariscal, T. Ma, J. Milovich, and R. Nora, *APS*, "Understanding 3D asymmetries in x-ray drive at the National Ignition Facility using a simple view factor metric," in 61st Annual Meeting of the APS Division of Plasma Physics, Vol. 64, No. 11, 21-25 October 2019 (Fort Lauderdale, FL, 2019), Abstract JO7.00010.
- <sup>19</sup>R. M. Bionta, G. P. Grim, K. D. Hahn, E. P. Hartouni, E. A. Henry, H. Y. Khater, A. S. Moore, and D. J. Schlossberg, "Real-time nuclear activation detectors for measuring neutron angular distributions at the National Ignition Facility," in Session T2H08 at High-Temperature Plasma Diagnostics, 14–17 December 2020.